Journal of Materials Chemistry C

Accepted Manuscript

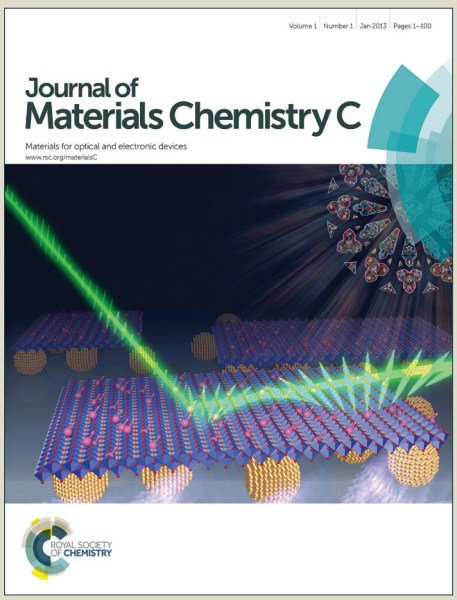

ROYAL SOCIETY OF CHEMISTRY

www.rsc.org/materialsC

Graphical and textual abstract

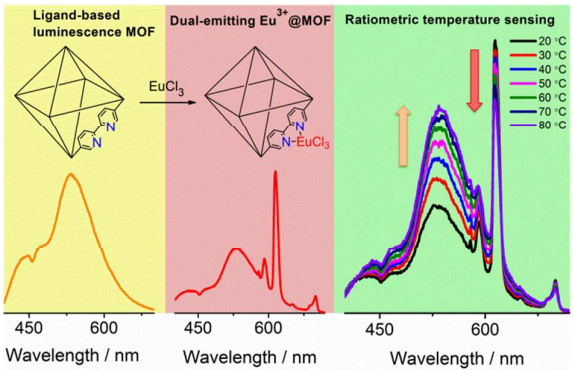

We herein describe a new strategy for the generation of ratiometric MOF thermometers, which is illustrated by imparting an additional lanthanide luminescence to a robust MOF with intrinsic ligand-based emission to form a dual-emissive hybrid for highly sensitive ratiometric temperature sensing

Journal Name

ARTICLE

Ratiometric detection of temperature with responsive dual-emissive MOF hybrids

Received 00th January 20xx,
Accepted 00th January 20xx

DOI: 10.1039/x0xx00000x

www.rsc.org/

You Zhou,[a] Bing Yan*[a]

Herein, we have developed a dual-emitting metal-organic framework (MOF) hybrid by imparting a addition lanthanide luminescence to a robust MOF with inherent broad emission. The imparted lanthanide emission is sensitized by the parented framework via energy transfer from the organic linkers embedded in the framework. The dual-emitting MOF hybrid exhibits an exactly contrary thermal dependence with respect to the intrinsic broad emision and incorperated lanthanide emisison, thus can serve as a robust platform for highly sensitive temperature sensing. This work represents a new approach for the generation of ratiometric MOF thermometers, as it highlights the opportunity of a variety of existing MOFs with inherent ligand-based or charge-transfer luminescence to explore ratiometric temperature sensing by the encapsulation of an additional lanthanide emission.

Introduction

Temperature is one of the most frequently measured variables as it pervades our description of the most basic of physical, chemical, and biological phenomena. By utilizing various kinds of temperature-dependent properties, such as volume, electric potential, electric conductance, IR emissivity, and photoluminescence, many types of thermometers have been developed for temperature measurement.[1] Of them, thermometers based on luminescent temperature-sensitive materials are gaining popularity due to their simplicity, noninvasive, high spatial and temporal resolution, and their ability to work even in biological fluids, strong electromagnetic fields and fast-moving objects.[2] So far, luminescence thermometers have primarily been done with organic dyes,[3] semiconductor nanocrystals,[4] lanthanides activated upconversion nanoparticles,[5] and lanthanide complexes.[6]

Luminescent metal-organic frameworks (MOFs) featuring permanent, well-defined porosity and intense fluorescence have emerged as very attractive functional hybrids in the past decades due to their applications in light-emitting devices and chemical sensors.[7] In addition, luminescent MOFs offer a new avenue for optical thermometry. The diverse luminescence and energy transfer processes within MOF materials make them well suited for designing fluorescent thermal probes. The early MOF thermometers are based on a single emission intensity which is responsive to temperature.[8] However, the accuracy of these intensity-based MOF thermometers is susceptible to errors introduced by optical occlusion, concentration inhomogeneities, excitation power fluctuations, or environment-induced nonradiative relaxation. To avoid these complications and give rise to a more robust self-referencing temperature sensing, Qian and co-workers developed a mixed lanthanide (Eu^{3+} and Tb^{3+}) MOF approach to fabricate ratiometric luminescence thermometer by taking advantage of the different thermal responses of Eu^{3+} and Tb^{3+} emissions.[9] By employing the same mixed lanthanide MOF approach, a variety of ratiometric MOF thermometers have been achieved.[10] Besides, Monge and coworkers engineered several different ratiometric thermometers operative in the cryogenic temperature region (80-240 K) by utilizing the phosphorescence of the ligand and lanthanide emissions of lanthanide MOFs ($Eu_{0.02}Gd_{0.98}$-DSB (DSB = 3,5-disulfobenzoate), $Tb_{0.02}Gd_{0.98}$-DSB, and $Eu_{0.05}Tb_{0.09}Gd_{0.86}$-DSB).[11] Recently, a new type of ratiometric thermometry was demonstrated in a dual-emissive MOF hybrid which obtained from encapsulating a perylene dye in the pores of a lanthanide MOF.[12] The ratiometric thermal detection of the hybrid relies on the temperature-dependent luminescence of both the lanthanide MOF and the incorporated perylene dye. The aforementioned three approaches are quite attractive to construct ratiometric thermal probes. Nevertheless, such approaches are limited by the lanthanide MOFs. So far, there have been no reports of the ratiometric optical thermometers constructed from MOFs with nonlanthanide luminescence (e.g., ligand-based or charge-transfer luminescence). Therefore, to exploit the nonlanthanide luminescent MOFs for ratiometric temperature sensing, an alternative way is desperately needed.

We herein describe a new strategy for the generation of ratiometric MOF thermometers, which is illustrated by imparting an additional lanthanide luminescence to a robust MOF with intrinsic ligand-based emission to form a dual-emissive hybrid for highly sensitive temperature sensing over the physiologic temperature range (Scheme 1a). The imparted emission is sensitized by the parented framework via energy transfer from the organic linkers

[a] Shanghai Key Lab of Chemical Assessment and Sustainability, Department of Chemistry, Tongji University, Siping Road 1239, Shanghai 200092, China. E-mail: byan@tongji.edu.cn;

† Electronic Supplementary Information (ESI) available. See DOI: 10.1039/b000000x/

ARTICLE Journal Name

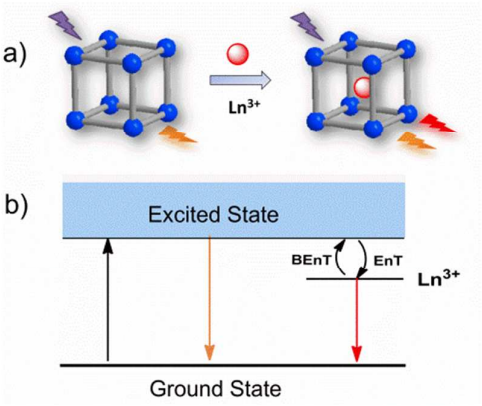

Scheme 1 (a) The schematic illustration of imparting an additional lanthanide emission to an intrinsic luminescence MOF to form dual emissive hybrid through postsynthetic functionalization. (b) The energy level structure of the dual emissive MOF. EnT and BEnT represent energy transfer and back energy transfer between organic linkers and Ln^{3+}, respectively.

embedded in the framework (Scheme 1b). The dual emissions of the hybrid have different thermal dependences, thus enabling their intensity ratio to be highly sensitive to the temperature. Our strategy paves the way for the nonlanthanide luminescence MOFs to explore ratiometric temperature sensing by the incorporation of an additional lanthanide emission.

Results and discussions

To demonstrate our strategy, we selected a robust UiO type framework, $Zr_6(\mu^3\text{-}O)_4(OH)_4(bpydc)_{12}$ (known as UiO-bpydc, bpydc = 2,2′-bipyridine-5,5′-dicarboxylic acid), for proof of principle. UiO-bpydc is characterized by the *fcu* structure with two types of cages (the octahedral cages with a diameter of 1.6 nm and the tetrahedral cages with a diameter of 1.2 nm).[13] UiO-bpydc was chosen for four reasons: (i) the inherent intense ligand-centered emission, (ii) the good thermal and chemical stability exposed to air, (iii) bipyridyl moieties were incorporated as free Lewis basic sites, thus can serve as scaffolds to anchor and sensitize lanthanide cations (Figure 1a), (iv) UiO-bpydc crystals can be tuned to nanoscale, which is beneficial for the applications in nanotechnology and biomedicine. The synthesis of UiO-bpydc was accomplished using a modified procedure from the literature.[13] The reaction of $ZrCl_4$ with H_2bpydc at 393 K for 24 h resulted in a white solid of UiO-bpydc. Powder X-ray diffraction pattern (PXRD) of the product was in good agreement with that simulated from the single crystal structure (Figure 1b).[13] The field emission scanning electron microscopy (FESEM) and transmission electron microscope (TEM) results revealed that the phase-pure product consists of homogeneous particles with crystal sizes in the range of 100-250 nm (Figure S1).

The postsynthetic functionalization of UiO-bpydc was performed by immersing the solid to a methanol solution of chlorine salts of Eu^{3+} (10^{-5} mol L^{-1}), which afford Eu^{3+}@UiO-bpydc hybrid. The crystallinity of UiO-bpydc was maintained in Eu^{3+}@UiO-bpydc as shown by their identical PXRD patterns (Figure 1b). The morphology and size of UiO-bpydc particles were also unchanged upon the

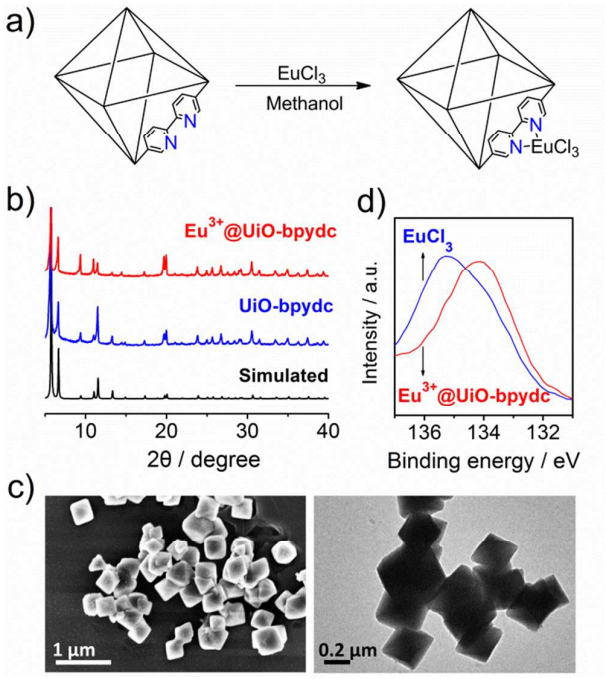

Figure 1 (a) Schematic representation of the postsynthetic Eu^{3+} functionalization of UiO-bpydc. (b) PXRD patterns of that simulated from the CIF file[12] (black), pristine UiO-bpydc (blue), and Eu^{3+}@UiO-bpydc (red). (c) Typical FESEM (left) and TEM (right) images of Eu^{3+}@UiO-bpydc particles. (d) Eu 4d XPS spectra of $EuCl_3$ (blue) and Eu^{3+}@UiO-bpydc (red).

incorporation of Eu^{3+} (Figure 1c). Inductively coupled plasma-mass spectrometry (ICP-MS) analyses of Zr/Eu ratios of the digested functionalized MOFs provided Eu loading of 0.1% for Eu^{3+}@UiO-bpydc. To determine the chemical states of Eu^{3+} in Eu^{3+}@UiO-bpydc, we recorded the Eu 4d X-ray photoelectron spectroscopy (XPS) core level spectra (Figure 1d). The Eu 4d XPS spectrum of Eu^{3+}@UiO-bpydc is similar to that of $EuCl_3$. However, its peak position (134.2 eV) shifts to a lower region in comparison with that of $EuCl_3$ (135.3 eV), suggesting that Eu^{3+} cations are coordinated to the free bipyridyl moieties embedded in UiO-bpydc as the coordinate covalent bond of Eu–N between Eu^{3+} and bipyridyl moieties will lead to an increase in the electron density of Eu^{3+} while a decrease in the binding energy.

The photoluminescence spectra of H_2bpydc and UiO-bpydc were examined at room temperature in the solid state. Upon 395 nm UV excitation, the free H_2bpydc ligand exhibits a strong and broad band with a maximum at 550 nm, which is originated from intraligand π-π* electron transition of H_2bpydc (Figure S2). The emission spectrum of UiO-bpydc is rather analogous to that of H_2bpydc ligand except for a slight blue shifting of the wavelength, providing an indication that the luminescence of the framework can be regarded as ligand-centered emission (Figure 2a). The blue-shift of the emission of bpydc within the MOF should be attributed to the deprotonation and coordination of H_2bpydc ligand to Zr^{4+} cations.

After the postsynthetic incorporation of Eu^{3+}, as expected, the product simultaneously shows both the intrinsic ligand-centered emission and characteristic sharp emissions of Eu^{3+} (Figure 2b). The

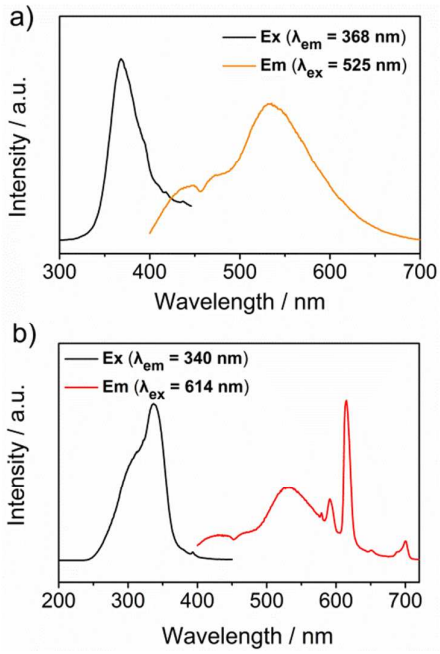

Figure 2 Room-temperature photoluminescence spectra of UiO-bpydc (a) and Eu^{3+}@UiO-bpydc (b) in the solid state.

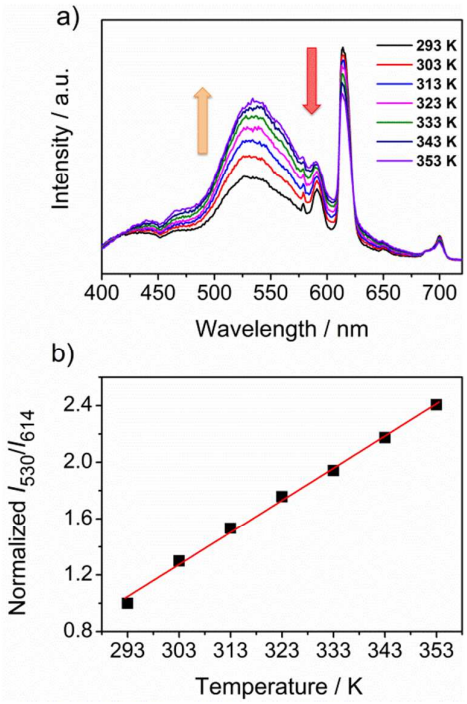

Figure 3 (a) Temperature-dependent emission spectra of Eu^{3+}@UiO-bpydc. (b) The intensity ratio of bpydc (530 nm) to Eu^{3+} (614 nm) as a function of temperature. Ratios were normalized to the value at 293 K.

luminescence of Eu^{3+} in Eu^{3+}@UiO-bpydc is sensitized by the bipyridyl moieties within the framework, which can be verified by the excitation spectrum collected for Eu^{3+}@UiO-bpydc at the monitoring wavelength of 614 nm. The intense broad band in the excitation spectrum peaking at 340 nm indicates the presence of energy transfer from the organic linkers to Eu^{3+} cations. The luminescence intensity of the Eu^{3+}@UiO-bpydc solid shows very little reduction as the time progresses, implying the good day to day fuorescence stability in air (Figure S3). Eu^{3+}@UiO-bpydc displays reasonably high decay time (521.3 us) and quantum yield (16.2%), implying that it can serve as excellent candidate for luminescence sensors. In addition, the relative intensity of ligand-centered emission to Eu^{3+} emission can be modulated by varying the content of the incorporated Eu^{3+}. As shown in Figure S4, upon increasing the loading level of Eu^{3+}, the characteristic emission of Eu^{3+} strengthens sharply, while the ligand-centered emission decreases to such a weak extent that it can hardly be observed due to the enhancement of the energy transfer probability from organic linkers to Eu^{3+}. Therefore, the Eu^{3+}@UiO-bpydc products with relative high Eu^{3+} contents don't possess the dual-emitting characteristic, thus are not available for ratiometric luminescence sensing.

To examine the feasibility of the Eu^{3+}@UiO-bpydc for ratiometric thermometry, the temperature-dependent photoluminescence properties were studied (Figure 3a). Eu^{3+}@UiO-bpydc exhibits an exactly contrary thermal dependence with respect to the emissions of bpydc linkers and Eu^{3+}. With the temperature rises, the Eu^{3+} emission intensity declines, while the ligand-centered emission significantly increases. To shed some light on the unique temperature-dependent luminescence behavior of Eu^{3+}@UiO-bpydc, the thermal responses of emissions of UiO-bpydc and $EuCl_3$ were determined for comparison. As illustrated in Figure S5, the broad band intensity of UiO-bpydc decreases as the increasing of temperature from 293 to 353 K owing to the thermal activation of nonradiative-decay pathways, which is a completely different scenario with that in Eu^{3+}@UiO-bpydc. Besides, the Eu^{3+} emission in $EuCl_3$ is insensitive to temperature. As shown in Figure S6, the luminescence intensity of $EuCl_3$ barely changed over the temperature range from 293 to 353 K. These results suggest that the significant luminescence enhancement of bpydc as well as the decrease in Eu^{3+} emission in Eu^{3+}@UiO-bpydc hybrid may be attributed to the back energy transfer (BEnT) from Eu^{3+} cations to bpydc linkers (Scheme 1b). Such BEnT process was further verified by the luminescence lifetime measurements. As presented in Figure S7, the decay time of Eu^{3+} reduced with the increase of temperature, while the decay time of the ligand emission slightly increased as the temperature elevates. In addition, the lifetime of ligand-based emission in UiO-bpydc monitored at 530 nm deceased as the temperature rises due to the thermal activation of nonradiative relaxation (Figure S7c), which is contrast to that in Eu^{3+}@UiO-bpydc composite. This phenomenon further verifies the back energy transfer process from Eu^{3+} to MOF. These results indicate the occurrence of the back energy transfer from Eu^{3+} to the bpydc linkers embedded in framework.

It is established that the thermal dependence of the BEnT rate follows an Arrhenius-type equation with an energy barrier E_a. To study the BEnT mechanism in detail, the energy back transfer rates

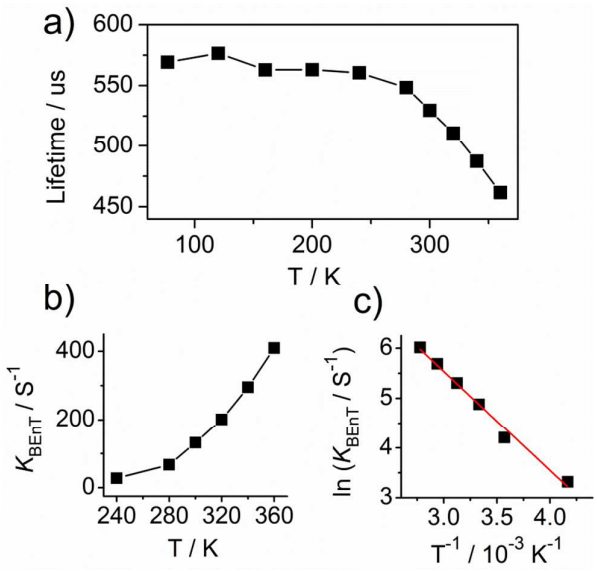

Figure 4. (a) Temperature-dependence of luminescence lifetime of Eu^{3+} in Eu^{3+}@UiO-bpydc. (b) Thermometric response curve plotting back energy transfer rate (K_{BEnT}) *vs.* temperature. (c) Arrehenius plots for back K_{BEnT} constants of Eu^{3+}@UiO-bpydc.

from Eu^{3+} to bpydc linkers (K_{BEnT}) were estimated by Arrhenius-type equation (1),[10e,14]

$$\ln K_{BEnT} = \ln (1/\tau - 1/\tau_0) = \ln A - E_a/RT \quad (1)$$

where τ is the luminescence lifetime of Eu^{3+} in Eu^{3+}@UiO-bpydc, τ_0 is the value at 77 K, A is the frequency factor, E_a is the activation energy, R is the gas constant, and T is the temperature. Temperature-dependent emission lifetimes (Eu^{3+}) of the MOF hybrid were recorded for the determination of K_b and E_a (Figure 4a). The calculated K_{BEnT} enhances with the increase of temperature, as presented in Figure 4b. The slope of Arrhenius plots for K_{BEnT} is 1.98, resulting in a value of 44 kJ mol^{-1} for activation energy E_a (Figure 4c).

To quantitatively determine the temperature sensing function of Eu^{3+}@UiO-bpydc, the ratiometric parameter was defined as the intensity ratio of 530 nm (bpydc) to 614 nm (Eu^{3+}) emission (I_{530}/I_{614}). Figure 3b plots the response of I_{530}/I_{614} (normalized to the 293 K value) to temperature in 10 K increment. We found I_{530}/I_{614} changed linearly with temperature in the range of 293-353 K. The linear relationship can be fitted as a function of

$$I_{530}/I_{614} = 0.592 + 0.0228T \quad (2)$$

with correlation coefficient (R^2) of 0.996, where T is the ambient temperature of Eu^{3+}@UiO-bpydc. Moreover, the thermal response of I_{530}/I_{614} is reversible between 293 and 353 K, as demonstrated by the temperature-dependent cycles of I_{530}/I_{614} ratios (Figure S8). The intensity ratios at different temperatures for each cycle are essentially the same, indicating the robustness of Eu^{3+}@UiO-bpydc as a thermometer. Figure S9 depicts the PXRD pattern and typical SEM images of Eu^{3+}@UiO-bpydc after multiple-run reversibility experiments. Both of them are essentially identical to that of fresh Eu^{3+}@UiO-bpydc, suggesting that Eu^{3+}@UiO-bpydc is stable for the duration of the three alternative thermo-cycles in the range of 293 and 353 K.

The thermometric sensitivity (S) of the Eu^{3+}@UiO-bpydc system was evaluated by the definition of

$$S(T) = \frac{\partial(I_{530}/I_{614})/\partial T}{I_{530}/I_{614}} \quad (3)$$

Figure S10 shows the calculated sensitivities of Eu^{3+}@UiO-bpydc within the range of 293-353 K. The maximum sensitivity of Eu^{3+}@UiO-bpydc is 2.99% K^{-1}, which can be comparable to that of the previously reported ratiometric MOF thermometers (Table S1). Moreover, the thermometric sensitivity of the MOF temperature probes developed by our strategy depends on the back energy transfer rates from incorporated Ln^{3+} cations to organic linkers embedded in MOF matrix. In principle, the back energy transfer rate can be modulated by utilizing different organic ligands of variable triplet state energy level (T1). Therefore, the thermometric sensitivity is expected to be enhanced and optimized by employing MOF matrixes with appropriate organic ligands.

In addition to the sensitivity, an important metric for measuring thermal probes is precision. With a perfect calibration curve, the precision of the luminescence thermometers depends only on the signal-to-noise ratios of the emission spectra. The error (SD) of the ratio I_{530}/I_{614} is determined as 6×10^{-3} from the data collected at temperatures over heating-cooling cycles (Figure S8), which translates to a precision of ± 0.26 K over the entire data set. Given a recent work showing subcellular temperature inhomogeneities of ~1 K, such Eu^{3+}@UiO-bpydc might be potentially useful in the biomedical diagnosis.[3b]

Conclusions

In conclusion, we developed a novel ratiometric thermometer by imparting an additional Eu^{3+} luminescence to a robust UiO-type MOF with intrinsic broad-band emission to yield the dual-emitting hybrid through a postsynthetic method. The unique energy transfer and back energy transfer processes between the two emitters in the hybrid endow the dual emissions with opposite thermal dependences, thus affording highly sensitive ratiometric temperature sensing. The maximum thermometric sensitivity is 2.99% K^{-1}, which is comparable to that of the previously reported MOF thermometers. The precision is determined as ± 0.26 K. This MOF hybrid self-calibrated thermometer with high sensitivity and precision, physiological operative range and submicrometer size is expected to have application in biomedicine. In addition, this work represents a new approach for the generation of ratiometric MOF thermometers, as it highlights the opportunity of a variety of existing MOFs with inherent ligand-based or charge-transfer luminescence to explore ratiometric temperature sensing by the incorporation of an additional lanthanide emission.

Experimental

Materials and methods

All chemicals were purchased from commercial sources and used without purification. $ZrCl_4 \cdot 4H_2O$ was purchased from Adamas. The ligand 2,2'-bipyridine-5,5'-dicarboxylic acid (H_2bpydc) was

purchased from Aldrich. Europium chloride was obtained from the corresponding oxides in HCl (37.5%).

Powder X-ray diffraction patterns (PXRD) were recorded with a Bruker D8 diffractometer using CuKα radiation with 40 mA and 40 kV. X-ray photoelectron spectroscopy (XPS) experiments were carried out on a RBD upgraded PHI-5000C ESCA system (Perkin Elmer) with MgKa radiation (*hv* = 1253.6 eV). Inductively coupled plasma-mass spectrometry (ICP-MS) data were collected on an X-7 series inductively coupled plasma-mass spectrometer (Thermo Elemental, Cheshire, UK), the samples were prepared by digesting the dry samples of Eu^{3+}@UiO-bpydc into concentrated HNO_3, followed by the dilution to 0.5% HNO_3 solution. The morphologies of samples were characterized by Field emission scanning electron microscopy (FESEM, Hitachi S4800). Transmission electron microscopy (TEM) was carried out using a JEOL JEM-2100F electron microscope and operated at 200 kV. The photoluminescence spectra and luminescent decay times were examined by an Edinburgh FLS920 phosphorimeter. The absolute external luminescent quantum efficiency was determined employing an integrating sphere (150 mm diameter, BaSO4 coating) from an Edinburgh FLS920 phosphorimeter.

Synthesis of UiO-bpydc

UiO-bpydc was prepared using a modified procedure from the literature.[1] The ligand 2,2'-bipyridine-5,5'-dicarboxylic acid (H_2bpydc, 0.248 g, 1 mmol), $ZrCl_4$ (0.233 g, 1 mmol), and glacial acetic acid (2.0 g, 33.33 mmol) were mixed in 60 ml DMF. Glacial acetic acid was added to provide better crystallinity of the product. After 30 minutes of stirring under ambient conditions, the mixture was transferred into a 100 ml Teflonlined stainless steel container and then heated at 393 K for 24 h. The resulting white solid was separated from the mixed dispersion by centrifugation and washed with DMF and methanol. To remove the organic species encapsulated within the pores of the open framework, the product was washed with methanol via Soxhlet extraction for 24 h, followed by drying at 333 K under vacuum.

Preparation of dual-emitting MOF hybrids

Dual-emitting Eu^{3+}@UiO-bpydc was prepared by immersing the UiO-bpydc solid (25 mg) in 5 mL ethanol solutions of chloride salts of Eu^{3+} (10^{-4} mmol) at 333 K for 24 h. The solid was then filtered off and soaked in 15 ml methanol. After 24 h, the supernatant was decanted and replaced by fresh methanol. This procedure was repeated two times to guarantee that the physically adsorbed $EuCl_3$ salt is removed. Finally, the product was collected by filtration and dried at 333 K under vacuum. The yield of Eu^{3+}@UiO-bpydc product based on UiO-bpydc was 91.3%. For the Eu^{3+}@UiO-bpydc products with higher Eu^{3+} contents, the feeding concentrations of $EuCl_3$ were 10^{-3} and 10^{-4} mmol, respectively.

Acknowledgements

This work was supported by the National Natural Science Foundation of China (91122003), Developing Science Funds of Tongji University and the Science & Technology Commission of Shanghai Municipality (14DZ2261100).

Notes and references

1 (a) P. R. N. Childs, J. R. Greenwood and C. A. Long, *Rev. Sci. Instrum.* 2000, **71**, 2959; (b) I. Suzuki, Rev. *Sci. Instrum.*, 1983, **54**, 868; (c) J. Seyedyagoobi, *Rev. Sci. Instrum.*, 1991, **62**, 249; (d) S. P. Wang, S. Westcott and W. Chen, *J. Phys. Chem. B*, 2002, **106**, 11203.

2 (a) X. D. Wang, O. S. Wolfbeis and R. J. Meier, *Chem. Soc. Rev.*, 2013, **42**, 7834; (b) Z. G. Yang, J. F. Cao, Y. X. He, J. H. Yang, T. Kim, X. J. Peng and J. S. Kim, *Chem. Soc. Rev.*, 2014, **43**, 4563; (c) E. J. McLaurin, L. R. Bradshaw and D. R. Gamelin, *Chem. Mater.*, 2013, **25**, 1283; (d) C. D. S. Brites, P. P. Lima, N. J. O. Silva, A. Millan, V. S. Amaral, F. Palacio and L. D. Carlos, *Nanoscale*, 2012, **4**, 4799.

3 (a) C. Gota, K. Okabe, T. Funatsu, Y. Harada and S. Uchiyama, *J. Am. Chem. Soc.*, 2009, **131**, 2766; (b) J. Feng, K. J. Tian, D. H. Hu, S. Q. Wang, S. Y. Li, Y. Zeng, Y. Li and G. Q. Yang, *Angew. Chem., Int. Edit.*, 2011, **50**, 8072; (b) K. Okabe, N. Inada, C. Gota, Y. Harada, T. Funatsu and S. Uchiyama, *Nat. Commun.*, 2012, **3**, 705; (c) F. M. Ye, C. F. Wu, Y. H. Jin, Y. H. Chan, X. J. Zhang and D. T. Chiu, *J. Am. Chem. Soc.*, 2011, **133**, 8146; (d) X. Liu, S. Y. Li, J. Feng, Y. Li and G. Q. Yang, *Chem. Commun.*, 2014, **50**, 2778; (e) C. Y. Chen and C. T. Chen, *Chem. Commun.*, 2011, **47**, 994;

4 (a) E. J. McLaurin, V. A. Vlaskin and D. R. Gamelin, *J. Am. Chem. Soc.*, 2011, **133**, 14978; (b) V. A. Vlaskin, N. Janssen, J. van Rijssel, R. Beaulac and D. R. Gamelin, *Nano Lett.*, 2010, **10**, 3670; (c) A. E. Albers, E. M. Chan, P. M. McBride, C. M. Ajo-Franklin, B. E. Cohen and B. A. Helms, *J. Am. Chem. Soc.*, 2012, **134**, 9565; (d) C. H. Hsia, A. Wuttig and H. Yang, *Acs Nano*, 2011, **5**, 9511; (e) S. L. Shinde and K. K. Nanda, *Angew. Chem., Int. Edit.*, 2013, **52**, 11325.

5 (a) M. L. Debasu, D. Ananias, I. Pastoriza-Santos, L. M. Liz-Marzan, J. Rocha and L. D. Carlos, *Adv. Mater.*, 2013, **25**, 4868. (b) A. Sedlmeier, D. E. Achatz, L. H. Fischer, H. H. Gorris and O. S. Wolfbeis, *Nanoscale*, 2012, **4**, 7090; (c) F. Vetrone, R. Naccache, A. Zamarron, A. J. de la Fuente, F. Sanz-Rodriguez, L. M. Maestro, E. M. Rodriguez, D. Jaque, J. G. Sole and J. A. Capobianco, *Acs Nano*, 2010, **4**, 3254.

6 (a) C. D. S. Brites, P. P. Lima, N. J. O. Silva, A. Millan, V. S. Amaral, F. Palacio and L. D. Carlos, *Adv. Mater.*, 2010, **22**, 4499; (b) H. S. Peng, M. I. J. Stich, J. B. Yu, L. N. Sun, L. H. Fischer and O. S. Wolfbeis, *Adv. Mater.*, 2010, **22**, 716; (c) Yuasa, R. Mukai, Y. Hasegawa and T. Kawai, *Chem. Commun.*, 2014, **50**, 7937; (d) C. D. S. Brites, P. P. Lima, N. J. O. Silva, A. Millan, V. S. Amaral, F. Palacio and L. D. Carlos, *New J. Chem.*, 2011, **35**, 1177; (e) A. Balamurugan, M. L. P. Reddy and M. Jayakannan, *J. Mater. Chem. A*, 2013, **1**, 2256; (f) Y. Takei, S. Arai, A. Murata, M. Takabayashi, K. Oyama, S. Ishiwata, S. Takeoka and M. Suzuki, *Acs Nano*, 2014, **8**, 198; (g) T. R. Wang, Peng Li and H. R. Li, *ACS Appl. Mater. Interfaces*, 2014, **6**, 12915.

7 (a) Q. B. Zhang, Y. J. Cui, Y. F. Yue, G. D. Qian and B. L. Chen, *Chem. Rev.*, 2012, **112**, 1126; (b) Z. C. Hu, B. J. Deibert and J. Li, *Chem. Soc. Rev.*, 2014, **43**, 5815; (c) Y. J. Cui, B. L. Chen and G. D. Qian, *Coord. Chem. Rev.*, 2014, **273**, 76; (d) J. Rocha, L. D. Carlos, F. A. A. Paz and D. Ananias, *Chem. Soc. Rev.*, 2011, **40**, 926.

8 (a) Q. R. Fang, G. S. Zhu, Z. Jin, Y. Y. Ji, J. W. Ye, M. Xue, H. Yang, Y. Wang and S. L. Qiu, *Angew. Chem., Int. Edit.*, 2007, **46**, 6638;

(b) Q. L. Zhu, T. L. Sheng, C. H. Tan, S. M. Hu, R. B. Fu and X. T. Wu, *Inorg. Chem.*, 2011, **50**, 7618; (c) Q. L. Zhu, C. J. Shen, C. H. Tan, T. L. Sheng, S. M. Hu and X. T. Wu, *Chem. Commun.*, 2012, **48**, 531;. (d) D. X. Ma, B. Y. Li, X. J. Zhou, Q. Zhou, K. Liu, G. Zeng, G. H. Li, Z. Shi and S. H. Feng, *Chem. Commun.*, 2013, **49**, 8964;

9 Y. J. Cui, H. Xu, Y. F. Yue, Z. Y. Guo, J. C. Yu, Z. X. Chen, J. K. Gao, Y. Yang, G. D. Qian and B. L. Chen, *J. Am. Chem. Soc.*, 2012, **134**, 3979.

10 (a) X. T. Rao, T. Song, J. K. Gao, Y. J. Cui, Y. Yang, C. D. Wu, B. L. Chen and G. D. Qian, *J. Am. Chem. Soc.*, 2013, **135**, 15559; (b) Y. J. Cui, W. F. Zou, R. J. Song, J. C. Yu, W. Q. Zhang, Y. Yang and G. D. Qian, *Chem. Commun*., 2014, **50**, 719; (c) A. Cadiau, C. D. S. Brites, P. M. F. J. Costa, R. A. S. Ferreira, J. Rocha and L. D. Carlos, *ACS Nano*, 2013, **7**, 7213; (d) Z. P. Wang, D. Ananias, A. Carne-Sanchez, C. D. S. Brites, I. Imaz, D. Maspoch, J. Rocha and L. D. Carlos, *Adv. Funct. Mater.*, 2015, **25**, 2824; (e) K. Miyata, Y. Konno, T. Nakanishi, A. Kobayashi, M. Kato, K. Fushimi and Y. Hasegawa, *Angew. Chem., Int. Ed.*, 2013, **52**, 6413; (f) Y. Q. Wei, R. J. Sa, Q. H. Li and K. C. Wu, *Dalton Trans.*, 2015, **44**, 3067; (g) Y. H. Han, C. B. Tian, Q. H. Li and S. W. Du, *J. Mater. Chem. C*, 2014, **2**, 8065; (h) Y. Zhou, B. Yan and F. Lei, *Chem. Commun.*, 2014, **50**, 15235; (i) Y. Zhou and B. Yan, *Nanoscale*, 2015, **7**, 4063; (j) X. Shen and B. Yan, *Dalton Trans.*, 2015, **44**, 1875.

11 R. F. D'Vries, S. Alvarez-Garcia, N. Snejko, L. E. Bausa, E. Gutierrez-Puebla, A. de Andres and M. A. Monge, *J. Mater. Chem. C*, 2013, **1**, 6316

12 Y. J. Cui, R. J. Song, J. C. Yu , M. Liu., Z. Q. Wang, C. D. Wu, Y. Yang, Z. Y Wang, B. L. Chen and G. D. Qian, *Adv. Mater.*, 2015, **27**, 1420.

13 L. J. Li, S. F. Tang, C. Wang, X. X. Lv, M. Jiang, H. Z. Wu and X. B. Zhao, *Chem. Commun.*, 2014, **50**, 2304.

14 G. Blasse, B. C. Grabmaier, *Luminescent materials*, Springer, New York, 1994, **92**.